Available online at www.sciencedirect.com
ScienceDirect
Analytical Biochemistry 365 (2007) 122–131
ANALYTICAL BIOCHEMISTRY
www.elsevier.com/locate/yabio

Nanocomposite of functionalized multiwall carbon nanotubes with nafion, nano platinum, and nano gold biosensing film for simultaneous determination of ascorbic acid, epinephrine, and uric acid

Umasankar Yogeswaran, Soundappan Thiagarajan, Shen-Ming Chen *

Department of Chemical Engineering and Biotechnology, National Taipei University of Technology, No. 1, Section 3, Chung-Hsiao East Road, Taipei 106, Taiwan, ROC

Received 27 January 2007
Available online 3 March 2007

Abstract

A unique bimetallic, nano platinum (Pt) with nano gold (Au) on nafion (NF) incorporated with functionalized multiwall carbon nanotubes (*f*-MWCNTs) composite film (*f*-MWCNTs–NF–PtAu) was developed by the potentiostatic method. The composite film exhibits promising efficient catalytic activity towards the oxidation of mixture of biochemical compounds and simultaneous measurement of ascorbate anion, epinephrine and urate anion in aqueous buffer solution (pH 6.75). Both, the cyclic voltammetry (CV) and differential pulse voltammetry (DPV) were used for the measurement of electroanalytical properties of neurotransmitters by means of composite film modified electrodes. Well-separated voltammetric peaks were obtained for ascorbate, epinephrine and urate anions with the peak separations of 0.222 and 0.131 V. The composite film can also be produced on gold and transparent semiconductor indium tin oxide electrodes for different kinds of studies such as electrochemical quartz crystal microbalance (EQCM), scanning electron microscopy (SEM), and atomic force microscopy (AFM). The incorporation of Pt and Au onto the *f*-MWCNTs–NF was revealed by the EQCM technique and the morphology of the film was studied using SEM, AFM and scanning electrochemical microscopy (SECM) techniques. Further, extensive studies were carried out using SECM for obtaining the surface current topographic images of composite film modified electrodes, and these indicated the presence of *f*-MWCNTs–NF–PtAu composite film on the electrode.
© 2007 Elsevier Inc. All rights reserved.

Keywords: Multiwall carbon nanotubes; Nano platinum; Nano gold; Composite film; Modified electrodes; Electrocatalysis; Vitamin C; Neurotransmitters

Electrochemically functional nanoparticles and carbon nanotubes (CNTs)[1] films have been of great interest for the past decade in electrocatalytic reactions because of their unique chemical and electrochemical properties. Previous studies revealed that intensive research has been carried out on the fabrication of sensor devices using nano platinum (Pt) and nano gold (Au) particles [1,2]. On the one hand, numerous methods have been used for the modification and application of Pt in electroanalysis; an example is the monolayers of phosphododecatungstate, where Pt tends to activate them towards the efficient electrocatalytic reduction of oxygen in acidic medium [3]. On the other hand, several steps have been taken to prepare nano Au using sol-gel, the dip-coating techniques for electrocatalysis applications. Willner and coworkers explored the possible use of an Au array for the construction of an electrochemical sensor with an extraordinary electrocatalytic property toward the electrochemical reduction of molecular oxygen in acidic media [4]. In addition, both Pt and Au were used for the selective

* Corresponding author. Fax: +886 2270 25238.
E-mail address: smchen78@ms15.hinet.net (S.-M. Chen).

[1] *Abbreviations used:* CNT, carbon nanotube; Pt, nano platinum; Au, nano gold; NF, nafion; GC, glassy carbon; AA, ascorbic acid; EP, epinephrine; UA, uric acid; SAM, self-assembled monolayer; *f*-MWCNTs, functionalized multiwall carbon nanotubes; SEM, scanning electron microscopy; AFM, atomic force microscopy; SECM, scanning electrochemical microscopy; CV, cyclic voltammetry; DPV, differential pulse voltammetry; EQCM, electrochemical quartz crystal microbalance; UME, ultramicroelectrode; ITO, indium tin oxide; LSV, linear sweep voltammetry.

0003-2697/$ - see front matter © 2007 Elsevier Inc. All rights reserved.
doi:10.1016/j.ab.2007.02.034

www.sprr.com.cn

determination of a few biochemical compounds [4–7]. Previously, the combinations of Pt and Au were prepared by chemical reduction of their corresponding metal complexes bound by the ion exchange [8] where, the method of size sorting was based on K_2BSPP [9]. However, CNTs showed interesting electrocatalytic activity for both bioorganic and inorganic compounds such as glutathione and IO_3^- [10–13]. In addition, CNTs were used for the methanol oxidation in the fuel cells, detection of insulin, and other biosensor applications. Their wide variety of applications has created great interest in the electrocatalysis field [14–16]. Even though the electrocatalytic activity of CNTs and nanoparticle films shows good results individually, some of the biochemical compounds do not undergo electrocatalysis. To overcome this difficulty, new studies have been developed for the preparation of composite films that were composed of both CNTs and nanoparticles. These composite films possess some unique interesting properties and enhanced electrocatalytic activity [17–19]. The rolled-up graphene sheets of carbon (i.e., CNTs) exhibit a π-conjugative structure with a highly hydrophobic surface. This unique property of the CNTs allows them to interact with some organic aromatic compounds through π–π electronic and hydrophobic interactions to form new structures [20–22]. Past attempts were made for the preparation of sandwiched films used in the designing of nanodevices with the help of noncovalent adsorption of enzyme and proteins on the side walls of CNTs, resulting in novel CNT-based nanostructures containing biochemical units [23–25]. Electrodes modified with composite films were widely used in capacitors, batteries, photoelectrochemistry, fuel cells, chemical sensors, and biosensors [26,27]. Besides CNTs and nanoparticles, there were other interesting polymer materials, one of which is nafion (NF). Due to the presence of a sulfonated group in NF and its strong acidic character, it has been used as a solid catalyst in organic synthesis. Extensive studies already have been carried out using hybrid thin films of CNTs–NF as well as Pt modified electrodes prepared by the electrodeposition of Pt on NF-coated glassy carbon (GC) electrode. Those film modified electrodes were used for the electrocatalytic oxidation of biochemical compounds [28–30].

Ascorbic acid (AA), as a constituent of the cell, has momentous biological functions and is an analyte of great importance because it is vital to immune response and wound healing [31]. It is found in fruits, vegetables, and beverages. Epinephrine (EP) is one of the important catecholamine neurotransmitters in the mammalian central nervous system and plays a very important role in the function of central nervous, renal, hormonal, and cardiovascular systems. Uric acid (UA) and other oxypurines are the principal final products of purine metabolism in the human body [32]. Abnormal levels of UA are symptoms of several diseases, including gout and hyperuricemia [33]. Furthermore, the catecholamine drugs are used to treat hypertension, bronchial asthma, and organic heart disease. They are used in cardiac surgery and in the treatment of myocardial infarction [34,35]. The oxidation of these compounds is interesting because this process occurs in the human body. However, AA, EP, and UA coexist in biological fluids such as blood and urine. Due to its crucial role in neurochemistry and industrial applications, several traditional methods have been used for its determination. Among these, electrochemical methods have more advantages over other methods in sensing the neurotransmitters in living organisms [36]. However, electrochemical analysis of unmodified electrodes, such as GC, has limitations because of the overlapping of oxidation potentials of AA, EP, and UA that often cause a pronounced fouling effect resulting in rather poor selectivity and reproducibility [37,38]. Previous attempts were made for the simultaneous determination of the neurotransmitters, such as the determination of EP in presence of UA or AA using meso-2,3-dimercaptosuccinic acid self-assembled Au and self-assembled monolayer (SAM) modified Au electrodes, respectively [39,40]. The simultaneous determination of AA and UA was also reported previously [41].

The literature clearly reveals that there were no previous attempts made for the synthesis of composite film composed of CNTs incorporating NF with Pt and Au. In this article, we report a novel composite film, *f*-MWCNTs–NF–PtAu, made of functionalized multiwall carbon nanotubes (*f*-MWCNTs) with NF, nano Pt, and nano Au as well as its characterization and enhanced catalytic activity towards biochemical compounds such as AA, EP, and UA, even at very low concentrations. The film formation processing involves modifying GC with uniformly well-dispersed *f*-MWCNTs aqueous solution, coating with a uniform thin layer of NF, and then electrochemically depositing bimetallic Pt and Au from an aqueous solution mixture. The morphology of the film was studied using the scanning electron microscopy (SEM), atomic force microscopy (AFM) and scanning electrochemical microscopy (SECM) methods. Initial studies showed that SECM is also a suitable technique for imaging *f*-MWCNTs–NF–PtAu because of its compatibility with the imaging parameters. This new electrochemical technique has shown great promise for studies of immobilized biomolecules with chemical and biological reactions at the electrode solution interface [42–44]. So, we also report here the SECM imaging of *f*-MWCNTs–NF–PtAu composite film by means of EP redox reaction.

Materials and methods

Apparatus

Cyclic voltammetry (CV) and differential pulse voltammetry (DPV) were performed in an analytical system model CHI-400 and CHI-900 potentiostat, respectively. A conventional three-electrode cell assembly, consisting of an Ag/AgCl reference electrode and a Pt wire counterelectrode, were used for the electrochemical measurements. The working electrode was either an unmodified GC or a GC modified with the composite films and all of the potentials were reported versus the Ag/AgCl reference electrode. The working electrode for electrochemical quartz crystal

www.sbm.com.cn

microbalance (EQCM) measurements was an 8 MHz AT-cut quartz crystal coated with a gold electrode. The diameter of the quartz crystal was 13.7 mm, and the diameter of the gold electrode was 5.0 mm. The morphological characterization of composite films was examined by means of SEM (S-3000H, Hitachi) and AFM (CSPM4000, Being Nano-Instruments). A commercial SECM (model 900, CH Instruments) was also used to control the tip potentials, obtain the approach curves, and measure the topographic current image of the composite film surface on the modified GC. A Pt ultramicroelectrode (UME) of 7 μm diameter was employed as an SECM tip. The auxiliary and reference electrode for the SECM measurement was a Pt wire and an Ag/AgCl (1 mol L^{-1} KCl) electrode. All of the measurements were carried out at 25 ± 2 °C.

Materials

K_2PtCl_6, $KAuCl_4.3H_2O$, NF, and MWCNTs (o.d. = 10–20 nm, i.d. = 2–10 nm, length = 0.5–200 μm) were obtained from Aldrich. AA, EP, and UA were obtained from Sigma–Aldrich and were used as received. All other chemicals used were of analytical grade. The preparation of aqueous solutions was done with doubly distilled deionized water. Solutions were deoxygenated by purging with prepurified nitrogen gas. Buffer solutions were prepared from 0.5 M H_2SO_4 and phosphate buffer (0.1 M NaH_2PO_4 and 0.1 M NaH_2PO_4) for the aqueous solutions (pH 6.75).

Fabrication of f-MWCNTs–NF and f-MWCNTs–NF–PtAu modified GCs

Difficulty in dispersing MWCNTs in a homogeneous aqueous solution was an important challenge in its preparation. Briefly, following previous studies, the functionalization of MWCNTs was done by weighing 10 mg of MWCNTs and 200 mg of potassium hydroxide in a Ruby Mortar and grained together for 2 h at room temperature (25 ± 2 °C). Then the reaction mixture was dissolved in 10 ml of doubly distilled deionized water and was precipitated many times in methanol for the complete removal of potassium hydroxide. The obtained *f*-MWCNTs with 10 ml water were ultrasonicated for 6 h to get a uniform dispersion. The functionalization of the MWCNTs was to obtain hydrophilic natured MWCNTs for complete homogeneous dispersion in water [45]. A homogeneous low-concentration NF solution was prepared by dissolving 1 ml of 5 wt% NF in 5 ml water.

Before starting each experiment, the GCs were polished by a BAS polishing kit with 0.05 μm alumina slurry, rinsed and then ultrasonicated in doubly distilled deionized water. The GCs studied were uniformly coated with 6.4 μg cm^{-2} (6 μl) of *f*-MWCNTs and dried, and then, 2 μl of NF was coated and dried at approximately 40 °C. The concentrations of homogeneously dispersed *f*-MWCNTs and NF were measured exactly using a microsyringe. The electrochemical deposition of nano Pt and nano Au was performed using electrochemical reduction of the mixture of K_2PtCl_6 and $KAuCl_4 \cdot 3H_2O$ (1×10^{-3} M and 2×10^{-3} M, respectively) on the *f*-MWCNTs–NF modified GCs in 0.5 M H_2SO_4 aqueous solution. It was performed by consecutive cyclic voltammograms over a suitable potential range of 1.5 to −0.15 V.

Results and discussion

Preparation of f-MWCNTs–NF–PtAu composite film and its electrochemical characterization

The adsorption of NF on *f*-MWCNTs and then the electrochemical deposition of the Pt and Au on *f*-MWCNTs–NF to form *f*-MWCNTs–NF–PtAu composite film are shown in Scheme 1. The bimetallic nanoparticles growth of the CV current corresponds to two reduction peaks for Pt and Au with the peak potentials $Ep_c = 0.27$ and 0.67 V, respectively, versus Ag/AgCl (see supplementary material). The oxidation peak potential of Au was $Ep_a =$ 1.05 V. The electrolyte solution used for electrodeposition was 0.5 M H_2SO_4 aqueous solution, which is highly acidic and facilitated the formation of nano-sized particles. The formal potential $E^{o\prime} = -0.09$ V shows the hydrogen adsorption and desorption because of the electrochemical reduction of Pt complex during nano Pt formation. On subsequent cycles, all the redox couples were found to be growing. These results indicated that during the cycle, the deposition of nano Pt and nano Au took place on GC surface at suitable positive potential scanning. Before other electrochemical characterizations, the prepared composite film was washed carefully in deionized water for removing H_2SO_4 that was present on the film. Then it was transferred to 0.1 M phosphate buffer aqueous solution (pH 6.75) for the other electrochemical characterizations in which the biochemical compounds were more stable. The cyclic voltammograms of *f*-MWCNTs–NF–PtAu composite film in phosphate buffer solution at different scan rates up to 200 mV s^{-1} (see supplementary material) show that the composite film formed in this way was stable at pH 6.75.

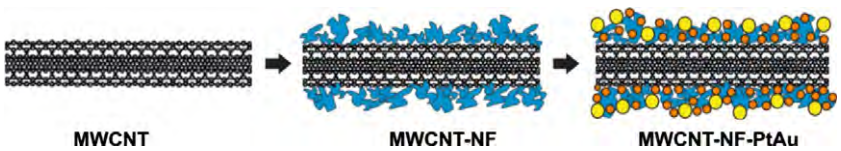

Scheme 1. Stepwise fabrication of *f*-MWCNTs–NF–PtAu composite film.

www.spm.com.cn

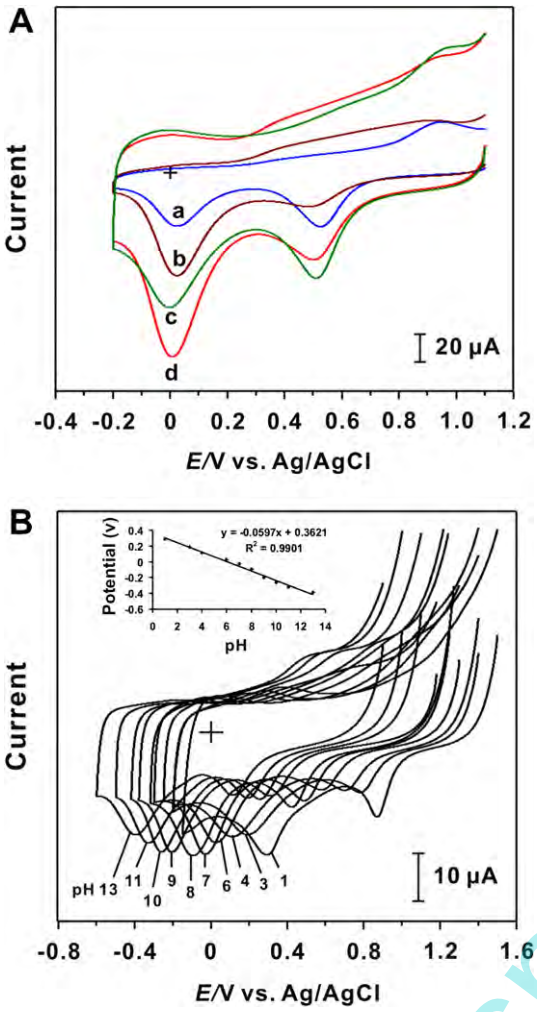

Fig. 1. (A) Cyclic voltammograms of NF–PtAu (a), PtAu (b), *f*-MWCNTs–NF–PtAu composite film (c) and *f*-MWCNT–PtAu (d) in 0.1 M phosphate aqueous buffer solution (pH 6.75). Scan rate: 100 mV s^{-1}. (B) Cyclic voltammograms of *f*-MWCNTs–NF–PtAu composite film synthesized in 0.5 M H_2SO_4 aqueous solution on GC and transferred to various pH solutions. The inset shows the formal potential versus pH.

The anodic and cathodic peak currents of the composite film redox couples increased linearly with the increase of scan rates up to 200 mV s^{-1}. This result demonstrated that the redox process was not controlled by diffusion up to 200 mV s^{-1}.

For a detailed comparison, the various films PtAu, NF–PtAu, *f*-MWCNTs–PtAu and *f*-MWCNTs–NF–PtAu, as shown in Fig. 1A, were prepared using 0.5 M H_2SO_4 aqueous electrolyte and were studied using the CV method in 0.1 M phosphate buffer solution (pH 6.75). The cyclic voltammogram of NF–PtAu film (Fig. 1A, curve a), with two peak currents of $Ip_c = 38.70$ and 39.78 μA for Pt and Au reduction, respectively, has a lower peak current magnitude than that of *f*-MWCNTs–NF–PtAu composite film. Curve b in Fig. 1A shows the cyclic voltammogram for nano PtAu film only, where $Ip_c = 75.0$ and 24.63 μA for Pt and Au, respectively. By comparing curves a and b in Fig. 1A, it is clear that the NF plays an important role in reducing the peak current magnitude of Pt, increasing the reduction peak current of Au, and balancing the reduction peak currents of both Pt and Au. Similar cases were also found in *f*-MWCNTs–NF–PtAu (curve c) and *f*-MWCNTs–PtAu (curve d). Among these, for curve c the $Ip_c = 98.30$ and 77.18 μA for Pt and Au, respectively, and for curve d the $Ip_c = 133.50$ and 63.07 μA for Pt and Au, respectively. Furthermore, in curves c and d, the magnitudes of the currents were higher than those of curves a and b. These results show that due to the large surface area of the *f*-MWCNTs, they play an important role in increasing the current magnitude and activity of the composite film. The oxidation peak current of Au, $Ip_a = -91.30$ μA, was also higher in curve c than in all other films. These results show that the *f*-MWCNTs and NF enhance the activity and the current magnitude of *f*-MWCNTs–NF–PtAu composite film. This unique *f*-MWCNTs–NF–PtAu composite film formed was characterized using electrochemical methods such as the CV, SECM, EQCM, and microscopic methods.

Fig. 1B shows the cyclic voltammograms of *f*-MWCNTs–NF–PtAu composite film synthesized in 0.5 M H_2SO_4 aqueous electrolyte and then washed with deionized water and transferred to various pH aqueous buffer solutions in the absence of K_2PtCl_6 and $KAuCl_4{\cdot}3H_2O$ mixture. These cyclic voltammograms reveal that the film was highly stable in the pH range between 1 and 13 and that the values of Ep_a and Ep_c depend on the pH value of the buffer solution. Perhaps the peaks involve an ion exchange; we suggest that the reduction currents of the composite film include a proton transfer. The inset in Fig. 1B shows the formal potential of *f*-MWCNTs–NF–PtAu composite film plotted over a pH range of 1 to 13 that has the slope of –60 mV/pH. This slope value is close to that given by the Nernstian equation for two electrons and two protons involved in the redox reaction.

Incorporation of Pt and Au onto f-MWCNTs–NF composite film through EQCM technique

The confirmation of the incorporation of Pt and Au onto *f*-MWCNTs–NF composite film was made using Fig. 2A, which shows the consecutive cyclic voltammograms and EQCM results for *f*-MWCNTs–NF–PtAu composite. The electrolyte solution used was 0.5 M H_2SO_4 containing the mixture of 1×10^{-3} M and 2×10^{-3} M of K_2PtCl_6 and $KAuCl_4{\cdot}3H_2O$, respectively. Fig. 2B indicates the change in the EQCM frequency recorded during the cycles of the consecutive cyclic voltammograms. The increase in voltammetric peak current of composite redox couple in Fig. 2A and the frequency decrease (or mass increase) in Fig. 2B were found to be consistent with the growth of Pt and Au film on the *f*-MWCNTs–NF modified gold electrode. These results also showed that the obvious deposition potential was started between 1.5 and –0.15 V. From the frequency change, the change in the mass in

www.spm.com.cn

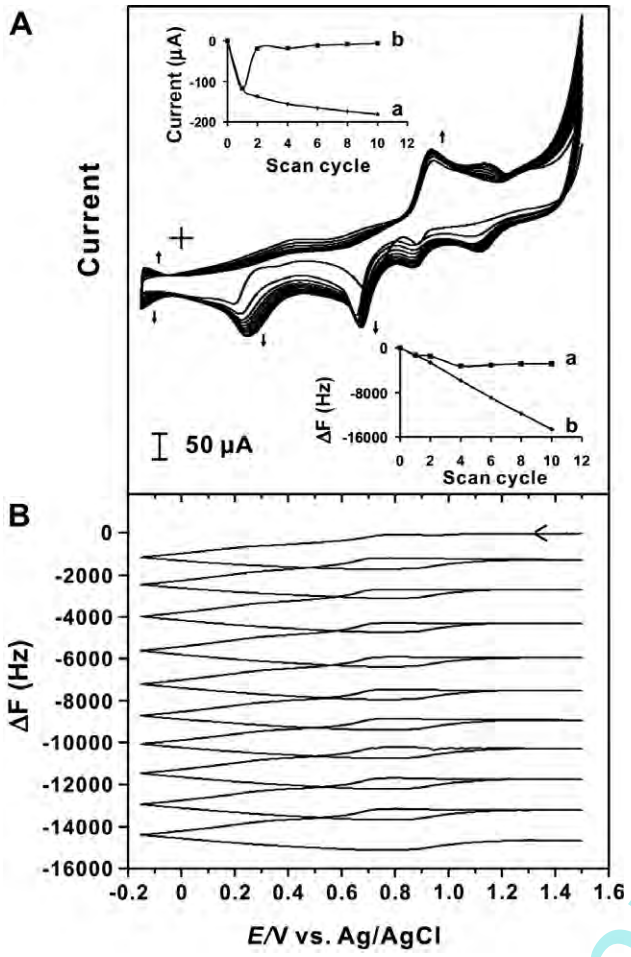

Fig. 2. (A) Consecutive potential cyclic voltammograms of a gold electrode modified from *f*-MWCNTs–NF–PtAu in 0.5 M H_2SO_4 aqueous solution. The upper inset shows a plot of cathodic peak current versus scan cycle (a) and every cycle of cathodic current change versus scan cycle (b). The lower inset shows a plot of every cycle frequency change ΔF versus scan cycle (a) and total frequency change ΔF versus scan cycle (b). (B) EQCM frequency change responses recorded together with the consecutive cyclic voltammograms between 1.5 and −0.15 V. Scan rate: 20 mV s^{-1}.

composite film at the quartz crystal can be calculated by the Sawerbery equation:

$$\text{Mass Change } (\Delta m) = -0.5(f_0^{-2})(\Delta f)A(K\rho)^{0.5} \quad (1)$$

where f_0 is the oscillation frequency of the crystal, Δf is the frequency change, A is the area of gold disk, and ρ is the density of the crystal. However, a 1-Hz frequency change is equivalent to 1.4 ng of mass change. The mass change during Pt and Au incorporation onto the *f*-MWCNTs–NF modified gold electrode for total cycles was found to be 20.51 μg cm^{-2}. The upper inset of Fig. 2A indicates the variation of cathodic peak current with the increase of the scan cycles (curve a) and every cycle of cathodic peak current with the increase of the scan cycles (curve b). The lower inset of Fig. 2A indicates the variation of every cycle of cathodic peak current with the increase of the scan cycles (curve a) and frequency change with the increase of the scan cycles (curve b). In Fig. 2A, curve a in the upper inset and curve b in the lower inset were found to be consistent with a linear change in the growth of Pt and Au on the *f*-MWCNTs–NF modified gold electrode. The modified gold electrode was carefully washed with deionized water, transferred to 0.1 M phosphate buffer aqueous solution (pH 6.75), and then scanned between −0.2 and 1.1 V (see supplementary material). By this EQCM result, the increase and decrease in frequency of the gold electrode during reduction and oxidation of Pt and Au were confirmed. Furthermore, the result reveals its property and its interaction with oxygen.

Topographic characterization of f-MWCNTs–NF–PtAu composite film using SEM, AFM, and SECM

NF–PtAu and *f*-MWCNTs–NF–PtAu composite films were prepared on indium tin oxide (ITO) with conditions and potential similar to that of GC and were characterized using the SEM and AFM techniques. The top SEM view of nanostructures of NF–PtAu in Fig. 3A on the ITO electrode shows that nano Pt and nano Au were formed as bright round-shaped, homogeneously dispersed particles adhering to the surface. Fig. 3B is the *f*-MWCNTs–NF–PtAu composite film on the ITO electrode and shows

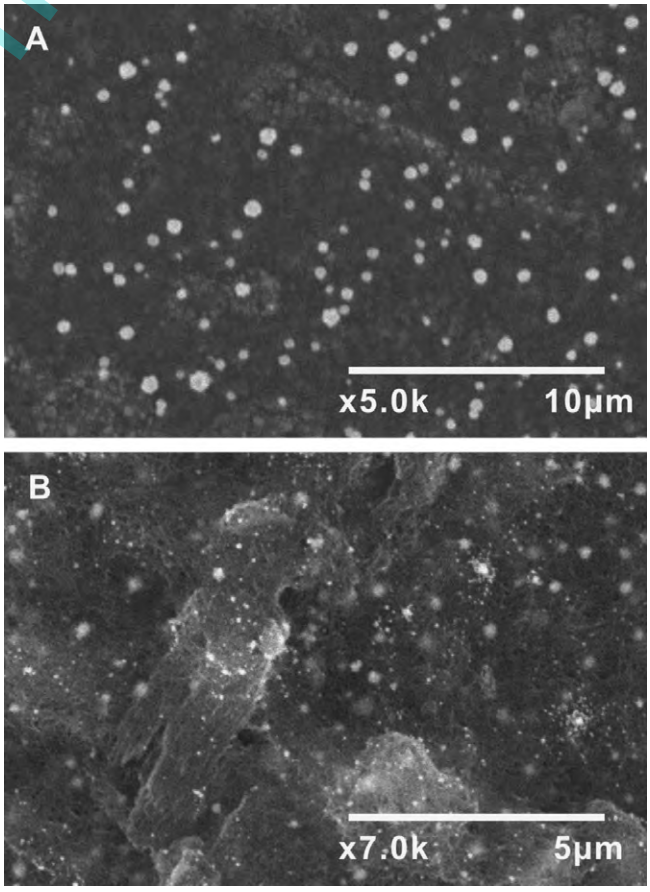

Fig. 3. SEM images of NF–PtAu (A) and *f*-MWCNTs–NF–PtAu composite film (B).

www.spm.com.cn

f-MWCNTs–NF with nano Pt and nano Au, an obvious formation of composite film. The image indicates that the particle size distributions of Pt and Au vary from 200 to 300 nm for Pt and from 50 to 80 nm for Au. Both the particles were distinguished by their size variation. Figs. 4A and B depict the surface topographic images of NF–PtAu and *f*-MWCNTs–NF–PtAu films, respectively, using the AFM technique. In Fig. 4A, the large and small particle structure formation shows the presence of both Pt and Au on the NF–PtAu film. From the horizontal cross section of the topographic images, we could clearly observe that the thickness of NF–PtAu was approximately 110 nm and that of *f*-MWCNTs–NF–PtAu was approximately 210 nm. These results, and a comparison of Figs. 4A and B, show the obvious formation of *f*-MWCNTs–NF–PtAu composite film. On the other hand, the three-dimensional view, phase, and amplitude of the surface also reveal that *f*-MWCNTs–NF–PtAu composite film is thicker than NF–PtAu film (see supplementary material). Finally, we could clearly observe the similarities between the SEM and AFM images for both of the films.

SECM experiments were carried out using 7 μm Pt UME in phosphate buffer aqueous solution (pH 6.75) containing 1×10^{-3} M EP as the redox mediator. The tip potential and substrate (*f*-MWCNTs–NF–PtAu) potential were held at −0.2 and 0.3 V, respectively, versus Ag/AgCl. Briefly, this technique was a scanning probe technique that was based on faradaic current changes as the UME tip was moved across the sample surface. The obtained images depend on the sample topography and surface reactivity. So, this technique could be used to examine differences in electrochemical activity on the surfaces at high resolution [46]. We were already aware that a frequent mode of operation for SECM is the feedback mode, where only the UME tip current is monitored. Fig. 5A depicts the positive and negative feedback probe approach curves for the *f*-MWCNTs–NF–PtAu film. Here the UME tip current is perturbed by the presence of a substrate at close proximity by blockage of the diffusion of the film to the tip (negative feedback) and by regeneration of the substrate (positive feedback). This effect allows investigation of both electrically insulating and conducting surfaces and makes possible imaging of the surfaces and the reactions that occur there. Figs. 5B and C show the SECM image and three-dimensional view of the *f*-MWCNTs–NF–PtAu, respectively, scanned over a 100×100 μm region using UME in close proximity to the modified electrode surface. Previously, similar results were shown for NF with CNT composite samples [47]. In contrast, the bright regions appearing in Fig. 5B represent higher UME tip current of the *f*-MWCNTs–NF–PtAu film, where the rate of EP regeneration was higher due to the facilitated electron communication properties of the composite film. The green region indicates the lower feedback current of the composite film area. The reaction mechanism for topographic imaging (Scheme 2B) can be explained by the reduction and regeneration of EP (oxidation product at the UME), whereas the tip approached the conductive substrate, leading to the positive feedback current at the UME tip. The three-dimensional view was used to clearly show and measure the high current regions of *f*-MWCNTs–NF–PtAu composite film. Here the current increase was due to the presence of *f*-MWCNT, NF, Pt, and Au in the composite film. Fig. 5D shows a cross-sectional view of the oxidation current of the *f*-MWCNTs–NF–PtAu film and depicts the film current in a particular area showing a broad curve and the other remaining as a straight line. These data indicate the higher and lower oxidation currents of EP at *f*-MWCNTs–NF–PtAu composite film modified electrode surface. These results show that by using EP as a redox mediator, we have scanned the topographic image of *f*-MWCNTs–NF–PtAu composite film by SECM and observed morphological structure similar to that of SEM and AFM topography.

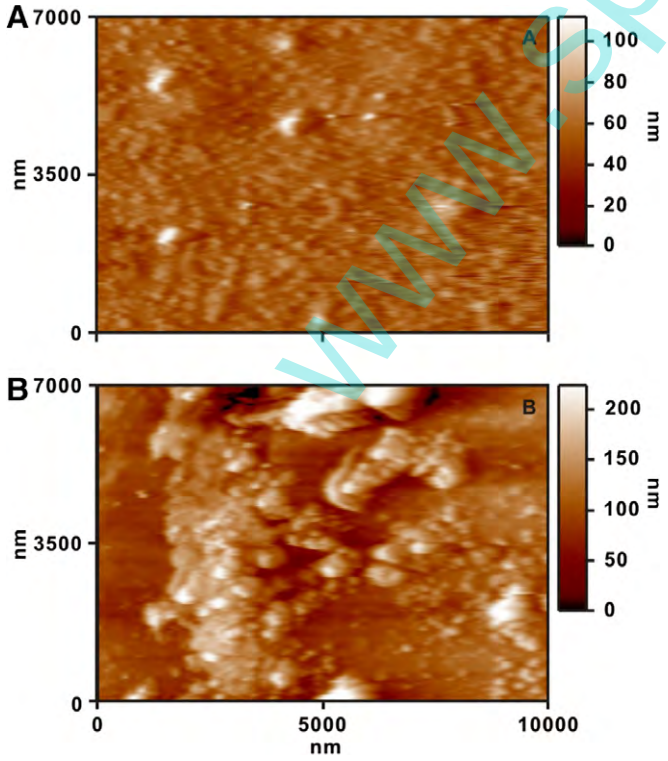

Fig. 4. AFM images of NF–PtAu (A) and *f*-MWCNTs–NF–PtAu composite film (B).

Voltammetric resolution and simultaneous determination of AA in the presence of EP and UA using CV and DPV

The electrocatalytic oxidations of AA, EP, and UA were performed separately, and the peak currents were found to be 0.03, 0.28, and 0.42 V, respectively (see supplementary material). The slopes of the linear calibration curves were used to calculate the sensitivity of *f*-MWCNTs–NF–PtAu composite film for AA, EP and UA in their respective analyte solutions (Table 1). Fig. 6 depicts the cyclic and differential pulse voltammograms obtained for AA, EP,

www.spm.com.cn

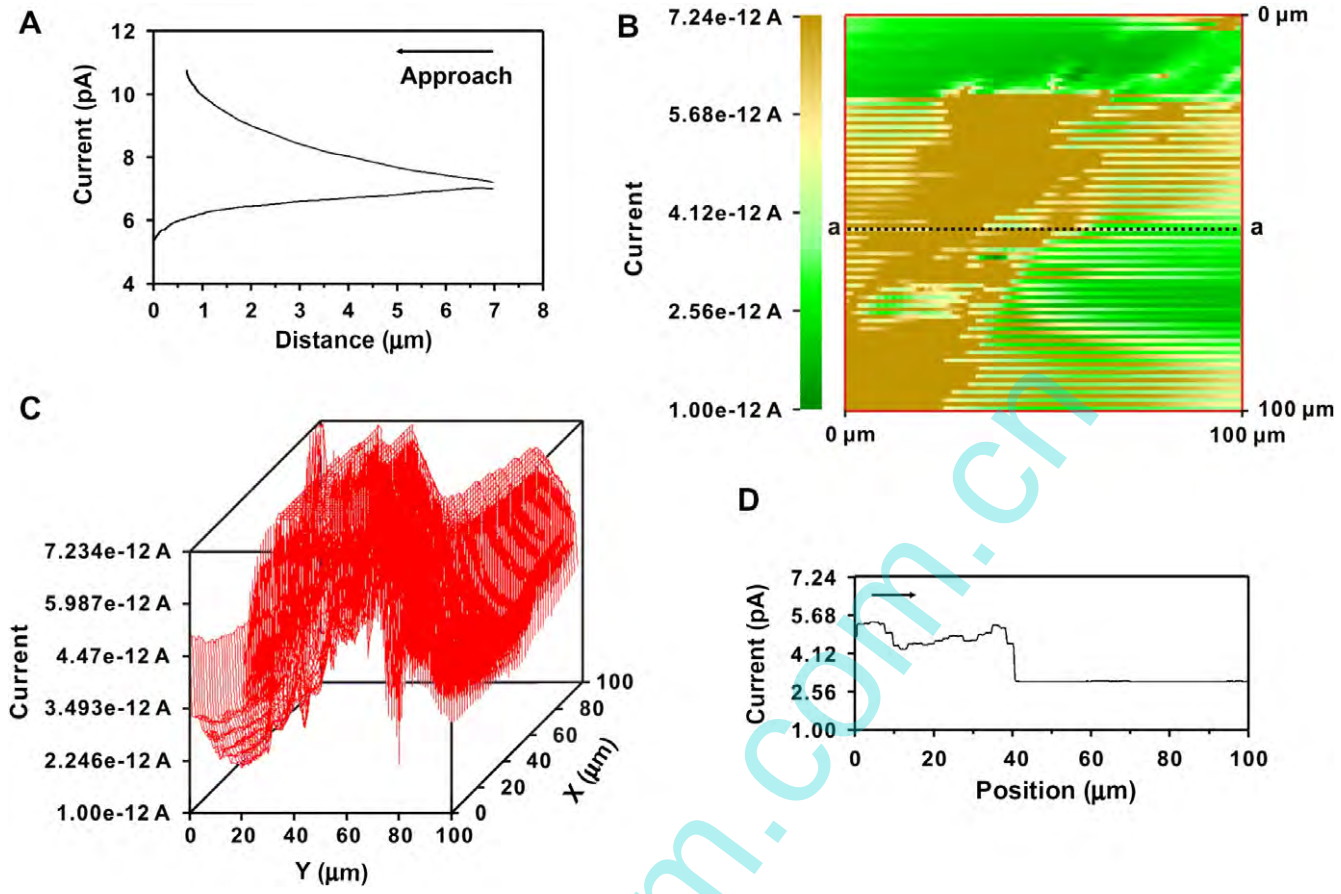

Fig. 5. (A) SECM approach curves obtained with 7 μm Pt UME tip moving toward modified *f*-MWCNTs–NF–PtAu surface. Electrolyte solution was EP in phosphate buffer (pH 6.75). (B) SECM images of surface of *f*-MWCNTs–NF–PtAu modified GC using 7 μm Pt UME tip in phosphate buffer (pH 6.75) containing EP as redox mediator. (C) Three-dimensional view of *f*-MWCNTs–NF–PtAu composite film modified GC. (D) Cross-sectional view of oxidation current along "a–a" dashed line shown in (B).

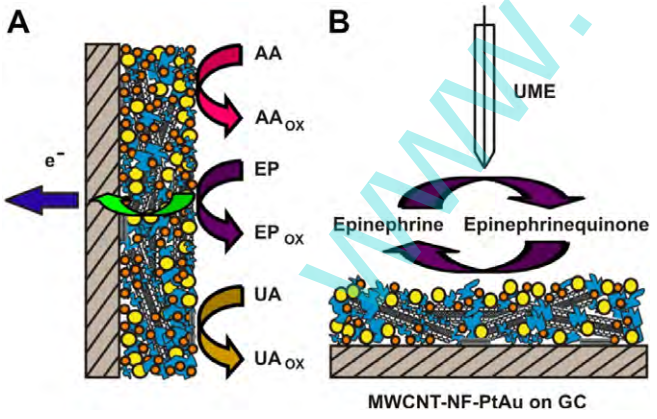

Scheme 2. Possible electrocatalytic reaction at *f*-MWCNTs–NF–PtAu in CV (A) and SECM (B).

and UA coexisting (AA+EP+UA mixture) at the bare and composite film modified GCs. The electrolyte used for electrocatalysis was 0.1 M phosphate buffer aqueous solution (pH 6.75), where the biochemical compounds are highly stable. Fig. 6A shows the cyclic voltammograms of the electrochemical oxidation of AA+EP+UA mixture at *f*-MWCNTs–NF–PtAu composite film and bare GC electrodes, with seven different individual concentrations of analytes in AA+EP+UA mixture. The cyclic voltammograms exhibited two reduction peaks and one oxidation peak for *f*-MWCNTs–NF–PtAu composite film in the absence of AA+EP+UA mixture. On the addition of AA+EP+UA mixture, three new increase in the oxidation peak for AA, EP, and UA appeared at $Ep_a = 0.07$, 0.29, and 0.42 V, respectively. The peak separation between AA and EP was 0.222 V, and the peak separation between EP and UA was 0.131 V. An increase in the concentration of AA+EP+UA mixture simultaneously produced an increase in the oxidation peak current of AA, EP, and UA with good film stability. The cyclic voltammograms on bare GC in Fig. 6A (curve a′) exhibited only one broad peak for AA+EP+UA mixture, the broad peak represents the voltammetric signals of AA, EP, and UA. Moreover, the peak current decreased in the subsequent cycles. These observations clearly indicated that the bare GC electrode failed to separate the voltammetric signals of AA, EP, and UA. The fouling effect of the electrode surface with the oxidized products of the analytes is the reason for obtaining the single peak for AA, EP, and UA in the

www.spm.com.cn

Table 1
Sensitivities and correlation coefficients of *f*-MWCNTs–NF–PtAu composite film for AA, EP, and UA individually and in AA+EP+UA mixture using different techniques

Type of technique	Sensitivity ($\mu A\ mM^{-1}$) and correlation coefficients[a]					
	AA[b]	EP[b]	UA[b]	AA in mixture[c]	EP in mixture[c]	UA in mixture[c]
CV	88.23 (0.977)	143.0 (0.939)	153.4 (0.962)	36.24 (0.983)	587.9 (0.940)	500.4 (0.972)
DPV	–	–	–	8.48 (0.904)	761.6 (0.903)	9.0 (0.942)

Note. Correlation coefficients are in parentheses.
[a] Where $n = 6$ for all of the data.
[b] Analytes from respective analyte solutions.
[c] Analytes from analyte mixture solution (AA+EP+UA).

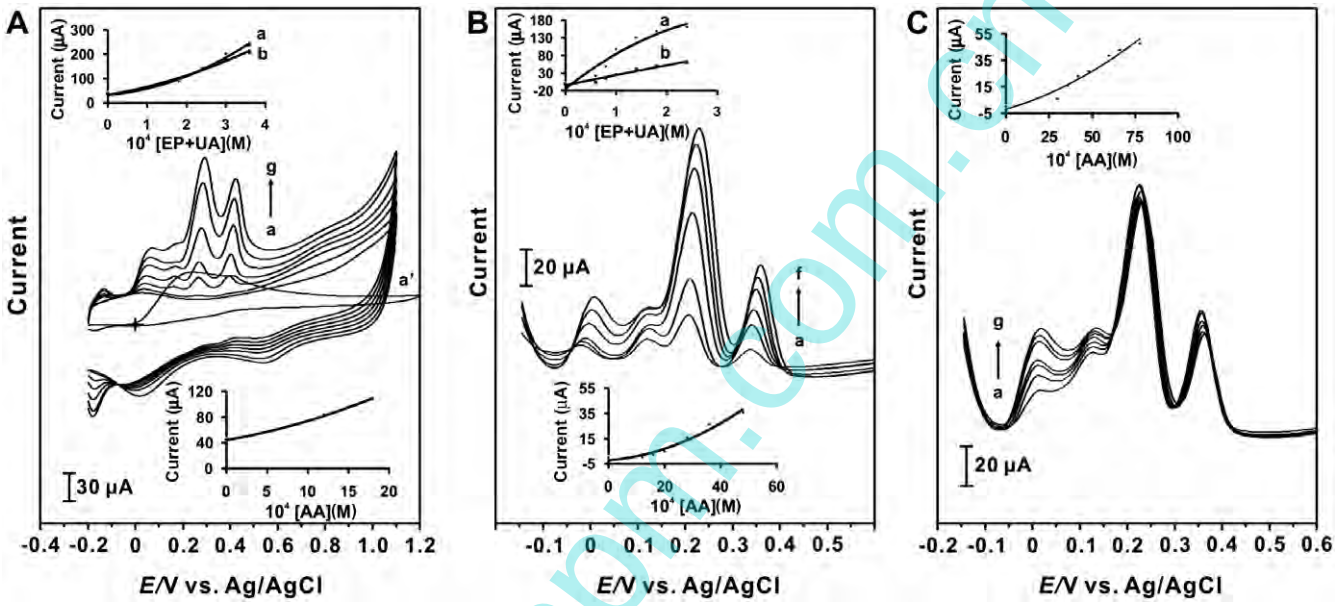

Fig. 6. (A) Cyclic voltammograms of *f*-MWCNTs–NF–PtAu composite film in 0.1 M phosphate aqueous buffer solution (pH 6.75) with various individual concentrations of analytes in AA+EP+UA mixture: bare GC with [AA and EP+UA] = 1.8×10^{-3} and 3.6×10^{-4} M (a′) and [AA and EP+UA] = 0.0 and 0.0 M (a); 3×10^{-4} and 6×10^{-5} M (b); 6×10^{-4} and 1.2×10^{-4} M (c); 9×10^{-4} and 1.8×10^{-4} M (d); 1.2×10^{-3} and 2.4×10^{-4} M (e); 1.5×10^{-3} and 3×10^{-4} M (f); 1.8×10^{-3} and 3.6×10^{-4} M (g). The upper inset shows the plot of current versus concentration of EP and UA at *f*-MWCNTs–NF–PtAu composite film with EP (a) and UA (b), and the lower inset shows the plot of current versus concentration of AA at *f*-MWCNTs–NF–PtAu composite film with AA. (B) Differential pulse voltammograms of *f*-MWCNTs–NF–PtAu composite film in 0.1 M phosphate aqueous buffer solution (pH 6.75) with various concentrations of AA and EP+UA: 1.2×10^{-3} and 6×10^{-5} M (a); 1.6×10^{-3} and 8×10^{-5} M (b); 2×10^{-3} and 1×10^{-4} M (c); 2.8×10^{-3} and 1.4×10^{-4} M (d); 3.6×10^{-3} and 1.8×10^{-4} M (e); 4.8×10^{-3} and 2.4×10^{-4} M (f). The upper inset shows the plot of current versus concentration of EP+UA at *f*-MWCNTs–NF–PtAu composite film with EP (a) and UA (b), and the lower inset shows the plot of current versus concentration of AA at *f*-MWCNTs–NF–PtAu composite film with AA. (C) Differential pulse voltammograms of *f*-MWCNTs–NF–PtAu composite film in 0.1 M phosphate buffer aqueous solution (pH 6.75) with various concentrations of AA in the presence of [EP+UA] = 4×10^{-4} M: [AA] = 3×10^{-3} M (a); 3.6×10^{-3} M (b); 4.2×10^{-3} M (c); 4.8×10^{-3} M (d); 6×10^{-3} M (e); 6.6×10^{-3} M (f); 7.8×10^{-3} M (g). The inset shows the plot of current versus concentration of AA at *f*-MWCNTs–NF–PtAu composite film with AA.

mixture [48]. The upper inset of Fig. 6A shows a plot of the concentration of EP and UA versus current at *f*-MWCNTs–NF–PtAu composite film, where curves a and b represent linear concentration increase of EP and UA in the solution mixture of three analytes. The lower inset of Fig. 6A shows a plot of the concentration of AA versus current at *f*-MWCNTs–NF–PtAu composite film, where the curve represents different concentrations of AA. From the slopes of those linear calibration plots, the sensitivity of *f*-MWCNTs–NF–PtAu composite film for AA, EP, and UA in AA+EP+UA mixture was calculated as shown in Table 1. Scheme 2A shows different possible interactions involved in the oxidation of AA, EP, and UA at *f*-MWCNTs–NF–PtAu composite modified electrode in 0.1 M phosphate buffer electrode (pH 6.75).

Fig. 6B shows the differential pulse voltammograms obtained at *f*-MWCNTs–NF–PtAu composite film modified electrode during the simultaneous change of the concentrations of AA+EP+UA mixture (curves a–f) at similar conditions. The differential pulse voltammograms were recorded at a constant time interval of 2 min with nitrogen purging before the start of each experiment. They demonstrated that the calibration curves for AA, EP, and UA were linear for a wide range of concentrations: 1.2 to 4.8 mM for AA and 0.06 to 0.24 mM for EP and UA. Even the lowest concentrations (0.02–0.16 mM for EP and UA)

www.spm.com.cn

were achieved by using linear sweep voltammetric (LSV) measurements (see supplementary material). These were one of the lowest and widest concentrations ever used for the detection of AA, EP, or UA in the aqueous solution. Interestingly, the peak currents for EP and UA increased linearly with the increase of EP and UA concentrations, whereas the peak current for AA did not increase. This phenomenon could have occurred due to the diffusion of EP and UA through the composite film being much faster compared than that of AA. Furthermore, in the EP oxidation case, it was supposed to be equal to the rate of diffusion for AA and UA; however, it is controversial. This can be explained as the electrostatic attractive effect between the positively charged EP species and the negatively charged fixed sites on the *f*-MWCNTs, facilitating the faster diffusion of EP into *f*-MWCNTs–NF–PtAu composite film. The upper inset of Fig. 6B is a plot of current versus concentration of EP and UA in AA+EP+UA mixture. The lower inset of Fig. 6B is a plot of current versus concentration of AA in AA+EP+UA mixture. By comparing these figures, the diffusion effect was clearly noticed. Those plots were also used for calculating the sensitivity of *f*-MWCNTs–NF–PtAu composite film using the DPV technique for the analytes in the mixture (Table 1). Fig. 6C exhibits the differential pulse voltammograms obtained for the different concentrations of AA (curves a–g) at *f*-MWCNTs–NF–PtAu composite film in the presence of a 0.4 mM concentration of EP and UA in the electrolyte solution. The voltammetric peak corresponding to the oxidation of AA increased linearly in consonance with the increase of the bulk concentration of AA, whereas the peak current for oxidation of EP and UA decreased slightly as the number of cycles increased. The inset of Fig. 6C is a plot of current versus concentration of AA in AA+EP+UA mixture, where the curve represents the concentration of AA in the solution mixture of three analytes. These results confirmed that the responses of AA, EP, and UA at *f*-MWCNTs–NF–PtAu composite film modified electrodes were independent.

Conclusions

We have developed a novel composite material with *f*-MWCNTs incorporated with nafion, nano Pt, and nano Au at the GC, gold, and ITO electrode surfaces in aqueous solution containing 0.5 M H_2SO_4 solution that was also highly stable in phosphate buffer aqueous solution (pH 6.75). The developed composite film for the simultaneous determination combines the advantages of ease of fabrication, high reproducibility, and sufficient long-term stability. The EQCM confirmed the incorporation of Pt and Au onto *f*-MWCNTs–NF modified GC. The SEM and AFM results confirmed the difference between the morphological data of NF–PtAu and *f*-MWCNTs–NF–PtAu composite films. The experimental method of CV and DPV with composite film biosensor integrated into a GC presented in this article provides an opportunity for qualitative and quantitative characterization and simultaneous determination of AA, EP, and UA at physiologically relevant conditions. The differential pulse voltammograms showed the oxidation currents of all three analytes and that they were not affected by the conditions of these three analytes coexisting in high concentrations. At the same time, the oxidized electrodes alleviated fouling problems, provided good repeatability of the voltammograms, and provided stability. The electrocatalysis of EP was also used in SECM for obtaining the topographic image of the composite film. Therefore, this work establishes and illustrates, in principle and potential, a simple and novel approach for the development of a simultaneous AA, EP, and UA voltammetric sensor that is based on the modified GC, ITO, and gold electrodes.

Acknowledgment

This work was supported by the National Science Council of the Taiwan, ROC.

Appendix A. Supplementary data

Supplementary data associated with this article can be found, in the online version, at doi:10.1016/j.ab.2007.02.034.

References

[1] O. Antoine, Y. Bultel, R. Durand, Oxygen reduction reaction kinetics and mechanism on platinum nanoparticles inside nafion, J. Electroanal. Chem. 499 (2001) 85–94.
[2] J. Jiang, A. Kucernak, Investigations of fuel cell reactions at the composite microelectrode solid polymer electrolyte interface: I. Hydrogen oxidation at the nanostructured PtNafion membrane interface, J. Electroanal. Chem. 567 (2004) 123–137.
[3] P.J. Kulesza, K. Karnicka, Network electrocatalytic films of conducting polymer-linked polyoxometallate-stabilized platinum nanoparticles, Electrochim. Acta 50 (2005) 5155–5162.
[4] A. Doron, E. Katz, I. Willner, Organization of Au colloids as monolayer films onto ITO glass surfaces: Application of the metal colloid films as base interfaces to construct redox-active monolayers, Langmuir 11 (1995) 1313–1317.
[5] K.C. Graber, G. Freeman, M.B. Hommer, M. Natan, Preparation and characterization of Au colloid monolayers, J. Anal. Chem. 67 (1995) 735–743.
[6] F.L. Leibowitz, W. Zheng, M.M. Maye, C. Zhong, Structures and properties of nanoparticle thin films formed via a one-step exchange–cross-linking–precipitation route, Anal. Chem. 71 (1999) 5076–5083.
[7] S. Senthil Kumar, J. Mathiyarasu, K.L. Phani, Exploration of synergism between a polymer matrix and gold nanoparticles for selective determination of dopamine, J. Electroanal. Chem. 578 (2005) 95–103.
[8] D.V. Ca, L. Sun, J.A. Cox, Optimization of the dispersion of gold and platinum nanoparticles on indium tin oxide for the electrocatalytic oxidation of cysteine and arsenite, Electrochim. Acta 51 (2006) 2188–2194.
[9] J.Y. Lee, H.P. Too, Size sorting of Au and Pt nanoparticles from arbitrary particle size distributions, Anal. Chim. Acta 546 (2005) 133–138.
[10] W. Zhang, F. Wan, W. Zhu, H. Xu, X. Ye, R. Cheng, L.T. Jin, Determination of glutathione and glutathione disulfide in hepato-

www.spm.com.cn

cytes by liquid chromatography with an electrode modified with functionalized carbon nanotubes, J. Chromatogr. B 818 (2005) 227–232.
[11] K. Gong, Y. Dong, S. Xiong, Y. Chen, L. Mao, Novel electrochemical method for sensitive determination of homocysteine with carbon nanotube-based electrodes, Biosens. Bioelectron. 20 (2004) 253–259.
[12] J. Chen, J. Bao, C. Cai, T. Lu, Electrocatalytic oxidation of NADH at an ordered carbon nanotubes modified glassy carbon electrode, Anal. Chim. Acta 516 (2004) 29–34.
[13] L. Qian, X. Yang, Composite film of carbon nanotubes and chitosan for preparation of amperometric hydrogen peroxide biosensor, Talanta 68 (2006) 721–727.
[14] G. Wu, Y.S. Chen, B.Q. Xu, Remarkable support effect of SWNTs in Pt catalyst for methanol electrooxidation, Electrochem. Commun. 7 (2005) 1237–1243.
[15] J. Wang, M. Musameh, Electrochemical detection of trace insulin at carbon-nanotube-modified electrodes, Anal. Chim. Acta 511 (2004) 33–36.
[16] J. Wang, M. Li, Z. Shi, N. Li, Z. Gu, Electrocatalytic oxidation of 3,4-dihydroxyphenylacetic acid at a glassy carbon electrode modified with single-wall carbon nanotubes, Electrochim. Acta 47 (2001) 651–657.
[17] Z. He, J. Chen, D. Liu, H. Zhou, Y. Kuang, Electrodeposition of Pt–Ru nanoparticles on carbon nanotubes and their electrocatalytic properties for methanol electrooxidation, Diamond Relat. Mater. 13 (2004) 1764–1770.
[18] H. Tang, J.H. Chen, Z.P. Huang, D.Z. Wang, Z.F. Ren, L.H. Nie, Y.F. Kuang, S.Z. Yao, High dispersion and electrocatalytic properties of platinum on well-aligned carbon nanotube arrays, Carbon 42 (2004) 191–197.
[19] J. Xu, K. Hua, G. Sun, C. Wang, X. Lv, Y. Wang, Electrooxidation of methanol on carbon nanotubes supported Pt–Fe alloy electrode, Electrochem. Commun. 8 (2006) 982–986.
[20] Q. Li, J. Zhang, H. Yan, M. He, Z. Liu, Thionine-mediated chemistry of carbon nanotubes, Carbon 42 (2004) 287–291.
[21] J. Zhang, J.K. Lee, Y. Wu, R.W. Murray, Photoluminescence and electronic interaction of anthracene derivatives adsorbed on sidewalls of single-walled carbon nanotubes, Nano Lett. 3 (2003) 403–407.
[22] A. Star, T.R. Han, J. Christophe, P. Gabriel, K. Bradley, G. Gruner, Interaction of aromatic compounds with carbon nanotubes: Correlation to the Hammett parameter of the substituent and measured carbon nanotube FET response, Nano Lett. 3 (2003) 1421–1423.
[23] R.J. Chen, Y. Zhang, D. Wang, H. Dai, Noncovalent sidewall functionalization of single-walled carbon nanotubes for protein immobilization, J. Am. Chem. Soc. 123 (2001) 3838–3839.
[24] M. Yang, Y. Yang, Y. Liu, G. Shen, R. Yu, Platinum nanoparticles-doped sol-gel/carbon nanotubes composite electrochemical sensors and biosensors, Biosens. Bioelectron. 21 (2006) 1125–1131.
[25] S.H. Lim, J. Wei, J. Lin, Electrochemical genosensing properties of gold nanoparticle–carbon nanotube hybrid, Chem. Phys. Lett. 400 (2004) 578–582.
[26] G.H. Deng, X. Xiao, J.H. Chen, X.B. Zeng, D.L. He, Y.F. Kuang, Controlled electrochemical oxidation for enhancing the capacitance of carbon nanotube composites, Carbon 43 (2005) 1557–1560.
[27] E. Frackowiak, V. Khomenko, K. Jurewicz, K. Lota, F. Béguin, Supercapacitors based on conducting polymers/nanotubes composites, J. Power Sources 153 (2006) 413–418.
[28] T. Selvaraju, R.R. Ramaraj, Electrochemically deposited nanostructured platinum on nafion coated electrode for sensor applications, J. Electroanal. Chem. 585 (2005) 290–300.
[29] M. Mao, D. Zhang, T. Sotomura, K. Nakatsu, N. Koshiba, T. Ohsaka, Mechanistic study of the reduction of oxygen in air electrode with manganese oxides as electrocatalysts, Electrochim. Acta 48 (2003) 1015–1021.
[30] M. Yasuzawa, A. Kunugi, Properties of glucose sensors prepared by the electropolymerization of a positively charged pyrrole derivative, Electrochem. Commun. 1 (1999) 459–462.
[31] G.F. Combs, The Vitamins: Fundamental Aspects in Nutrition and Health, 2nd ed., Academic Press, San Diego, 1992.
[32] G. Dryhurst, Electrochemistry of Biological Molecules, Academic Press, New York, 1977.
[33] J.M. Zen, J.J. Jou, G. Ilangovan, Selective voltammetric method for uric acid detection using pre-anodized nafion-coated glassy carbon electrodes, Analyst 123 (1998) 1345–1350.
[34] M.H. Sorouraddin, J.L. Manzoori, E. Kargarzadeh, A.M.H. Shabani, J. Pharm, Spectrophotometric determination of some catecholamine drugs using sodium bismuthate, Biomed. Anal. 18 (1998) 877–881.
[35] M.E. El-Kommos, F.A. Mohamed, A.S.K. Khedr, Spectrophotometric determination of some catecholamine drugs using metaperiodate, J. Assoc. Off. Anal. Chem. 73 (1990) 516–520.
[36] B.J. Venton, R.M. Wightman, Psychoanalytical electrochemistry: Dopamine and behavior, Anal. Chem. 1 (2003) 414A–421A.
[37] J. Chen, C.S. Cha, Detection of dopamine in the presence of a large excess of ascorbic acid by using the powder microelectrode technique, J. Electroanal. Chem. 463 (1999) 93–99.
[38] M.A. Dayton, A.G. Ewing, R.M. Wightman, Response of microvoltammetric electrodes to homogeneous catalytic and slow heterogeneous charge-transfer reactions, Anal. Chem. 52 (1980) 2392–2396.
[39] Y.X. Sun, S.F. Wang, X.H. Zhang, Y.F. Huang, Simultaneous determination of epinephrine and ascorbic acid at the electrochemical sensor of triazole SAM modified gold electrode, Sens. Actuat. B 113 (2006) 156–161.
[40] N.B. Li, L.M. Niu, H.Q. Luo, Electrochemical behavior of uric acid and epinephrine at a meso-2,3-dimercaptosuccinic acid self-assembled gold electrode, Microchim. Acta 153 (2006) 37–44.
[41] J. Premkumar, S.B. Khoo, Electrocatalytic oxidations of biological molecules (ascorbic acid and uric acid) at highly oxidized electrodes, J. Electroanal. Chem. 576 (2005) 105–112.
[42] F.R.F. Fan, A.J. Bard, Varieties of imaging with scanning probe microscopes, Proc. Natl. Acad. Sci. USA 96 (1999) 14222–14227.
[43] K. Yamashita, M. Takagi, K. Uchida, H. Kondo, S. Takenaka, Visualization of DNA microarrays by scanning electrochemical microscopy (SECM), Analyst 126 (2001) 1210–1211.
[44] J. Wang, F. Song, F. Zhou, Silver-enhanced imaging of DNA hybridization at DNA microarrays with scanning electrochemical microscopy, Langmuir 18 (2002) 6653–6658.
[45] Y. Yan, M. Zhang, K. Gong, L. Su, Z. Guo, L. Mao, Adsorption of methylene blue dye onto carbon nanotubes: A route to an electrochemically functional nanostructure and its layer-by-layer assembled nanocomposite, Chem. Mater. 17 (2005) 3457–3463.
[46] D.O. Wipf, A.J. Bard, Scanning electrochemical microscopy, J. Electrochem. Soc. 138 (1991) 469–474.
[47] H.S. Wang, T.H. Li, W.L. Jia, H.Y. Xu, Highly selective and sensitive determination of dopamine using a nafion/carbon nanotubes coated poly(3-methylthiophene) modified electrode, Biosens. Bioelectron. 22 (2006) 664–669.
[48] C.R. Raj, K. Tokuda, T. Ohsaka, Electroanalytical applications of cationic self-assembled monolayers: Square-wave voltammetric determination of dopamine and ascorbate, Bioelectrochemistry 53 (2001) 183–191.

www.spm.com.cn